

# Inferring hydroxyl layer peak heights from ground-based measurements of OH(6-2) band integrated emission rate at Longyearbyen (78° N, 16° E)

F. J. Mulligan<sup>1</sup>, M. E. Dyrland<sup>2</sup>, F. Sigernes<sup>2</sup>, and C. S. Deehr<sup>3</sup>

<sup>1</sup>National University of Ireland Maynooth, Ireland

<sup>2</sup>The University Centre in Svalbard, Norway

<sup>3</sup>University of Alaska Fairbanks, USA

Received: 23 June 2009 – Revised: 20 October 2009 – Accepted: 29 October 2009 – Published: 6 November 2009

**Abstract.** Measurements of hydroxyl nightglow emissions over Longyearbyen (78° N, 16° E) recorded simultaneously by the SABER instrument onboard the TIMED satellite and a ground-based Ebert-Fastie spectrometer have been used to derive an empirical formula for the height of the OH layer as a function of the integrated emission rate (IER). Altitude profiles of the OH volume emission rate (VER) derived from SABER observations over a period of more than six years provided a relation between the height of the OH layer peak and the integrated emission rate following the procedure described by Liu and Shepherd (2006). An extended period of overlap of SABER and ground-based spectrometer measurements of OH(6-2) IER during the 2003–2004 winter season allowed us to express ground-based IER values in terms of their satellite equivalents. The combination of these two formulae provided a method for inferring an altitude of the OH emission layer over Longyearbyen from ground-based measurements alone. Such a method is required when SABER is in a southward looking yaw cycle. In the SABER data for the period 2002–2008, the peak altitude of the OH layer ranged from a minimum near 76 km to a maximum near 90 km. The uncertainty in the inferred altitude of the peak emission, which includes a contribution for atmospheric extinction, was estimated to be  $\pm 2.7$  km and is comparable with the  $\pm 2.6$  km value quoted for the nominal altitude (87 km) of the OH layer. Longer periods of overlap of satellite and ground-based measurements together with simultaneous on-site measurements of atmospheric extinction could reduce the uncertainty to approximately 2 km.

**Keywords.** Atmospheric composition and structure (Airglow and aurora; Middle atmosphere – composition and chemistry; Instruments and techniques)

## 1 Introduction

An Ebert-Fastie spectrometer has been used to record spectra of hydroxyl nightglow emissions (OH(6-2) and OH(8-3) bands) at Longyearbyen (78° N, 16° E) in each winter season for more than 20 years. Analysis of these spectra has provided a detailed record of the rotational temperature at the altitude from which the emissions originate (e.g., Sivjee and Hamwey, 1987; Sivjee et al., 1987; Sigernes et al, 2003; Dyrland and Sigernes, 2007). These measurements have always been subject to the twin difficulties of an inexact knowledge of the emission height and the dependence of the retrieved temperature on the rotational transition probabilities. The work reported here concentrates on the question of the emission height only. Following the work of Baker and Stair (1988), the OH layer has been considered to be represented by an  $\sim 8$  km layer centred at 87 km altitude. Subsequent reports by She and Lowe (1998) and Oberheide et al. (2006) have confirmed that this interpretation is an accurate assessment of the time averaged height and width of the layer. A more detailed study by Yee et al. (1997) using HRDI (High Resolution Doppler Imager) results from UARS (Upper Atmosphere Research Satellite) showed that the peak altitude of the night time OH emissions could occur anywhere in the range 86–91 km. HRDI observations showed an inverse relationship between the nightglow brightness and peak emission altitude. Liu and Shepherd (2006) using OH volume emission rate (VER) data from the WINDII (Wind Imaging



Correspondence to: F. J. Mulligan  
(frank.mulligan@nuim.ie)

Interferometer) instrument on board the UARS satellite reaffirmed the inverse relationship and reported systematic variations in the peak altitude of the OH layer between 40° S and 40° N. High latitude observations were precluded by the inclination of the UARS spacecraft orbit. Using data from the SABER (Sounding of the Atmosphere by Broadband Emission Radiometry) instrument on the TIMED (Thermosphere Ionosphere Mesosphere Energetics and Dynamics) satellite, Winick et al. (2009) found that in the region poleward of 60° N, the OH layer was between 5 km and 8 km lower than normal during the boreal winters of 2004 and 2006. Changes in altitude of this magnitude together with the associated adiabatic heating/cooling will result in substantial temperature variations, the interpretation of which is eased considerably if OH emission height information is available. Takahashi et al. (2005) have called for further investigations of the relation of temporal variation between hydroxyl emission rates, height and temperatures.

Knowledge of the OH emission height is also important because of the role of OH temperature measurements in the assignment of temperatures derived from meteor radars in the MLT region. Meteor radar temperatures offer the possibility of 24 h per day measurements and in all sky conditions (Hocking et al., 2007). Hall et al. (2004) extrapolated the OH temperatures from 87 km to 90 km for the purpose of a multi-instrument derivation of 90 km temperatures over Svalbard based on the CIRA-86 and MSISE-90 models. A similar extrapolation technique based on MSIS-00 was employed by the same authors in 2006 (Hall et al., 2006). The validity of their meteor derived temperatures depends on the assumption that the OH layer is centred on 87 km altitude. Interpretation of rotational temperatures derived from OH emissions must, therefore, take account of the altitude of the emitting layer.

A number of recent reports have sought to infer the altitude of the peak of OH emission by combining results from different ground-based instruments. Employing a pair of all-sky imagers at sites 32 km apart, Kubota et al. (1999) observed common features in nightglow structure and found that the inverse relationship between brightness and altitude persisted on a local scale. Takahashi et al. (2005) reported OH emission heights deduced from cross correlating rotational temperatures from the OH(6-2) band and meteor trail ambipolar diffusion coefficients at Shigaraki (35° N, 136° E). Kumar et al. (2008) employed a similar technique to infer day-time emission heights over Thumba (8.5° N, 77° E) which corresponded well with peak heights observed in SABER OH VER profiles in the same time period. Liu and Shepherd (2006) found that, in the latitude range 40° S to 40° N, the altitude of the peak of the OH layer is almost completely described by the integrated emission rates (IER) in their study of WINDII profiles from the UARS satellite. Ground-based instruments that collect photons from all altitudes in the OH layer within their field of view are well suited for measuring IER and offer the possibility to assign an altitude to each ground-based measurement. Of course ground-based IER

measurements are subject to the effects of atmospheric extinction, which does not apply in the case of satellite observations. At 78° N, Longyearbyen is outside the range of latitude covered by the study of Liu and Shepherd (2006) and of the WINDII measurements. The SABER instrument measures broadband emission in the range 1.56–1.72  $\mu\text{m}$ , which includes mostly the OH(4-2) and (5-3) band from which OH VER profiles are calculated via an inversion technique, and provides excellent coverage at 78° N during northward looking yaw cycles. Unfortunately, SABER is in its southward looking phase during a large part of the Arctic winter season (mid-November–mid-January) when its latitude coverage does not extend above 54° N.

A remarkable period of good observing conditions during the winter of 2003/2004 provided 35 days (16 January–19 February) of measurements of OH emissions by the ground-based Ebert-Fastie spectrometer at Longyearbyen during a time when the SABER instrument was in a northward looking yaw cycle. This allowed us to establish a relation between the OH IER derived from the satellite observations and the OH(6-2) IER measured by the spectrometer. The remainder of this paper reports our efforts to adapt the procedure described by Liu and Shepherd (2006) to SABER OH VER profiles and to relate the empirical formula thus obtained to the OH(6-2) IER measured by the Ebert-Fastie spectrometer deployed at Longyearbyen. The purpose was to infer hydroxyl layer peak heights during periods when SABER is in a southward looking yaw cycle.

## 2 Data and analysis

### 2.1 SABER on TIMED

Liu and Shepherd (2006) made use of more than 50 000 altitude profiles of volume emission rate (VER) collected by WINDII for the OH(8-3) band P<sub>1</sub>(3) line emission to derive an empirical formula for the altitude of the OH nightglow emission. The results were formulated in terms of zonal averages covering the latitude range 40° S to 40° N. The work reported here makes use of OH VER altitude profiles derived from observations by the SABER instrument on board NASA's TIMED satellite. SABER measures vertical Earth limb emission profiles in 10 broadband spectral channels covering the wavelength range 1.27  $\mu\text{m}$  to 17  $\mu\text{m}$  (Mertens et al., 2004). The high inclination angle of TIMED's orbit (74 degrees to the equator) allows it to observe tangent points as far north as Longyearbyen, when it is in a northward looking yaw cycle. The TIMED satellite orbits the Earth about 15 times per day, and measures about 100 limb profiles in each orbit. SABER has a vertical resolution of approximately 2 km in the altitude range 10–105 km, and an along track resolution of near 400 km. OH VER profiles of the OH-B ( $\sim 1.6 \mu\text{m}$ ) channel from SABER Level 2A data (version 1.07) (available at <http://saber.gats-inc.com>) were

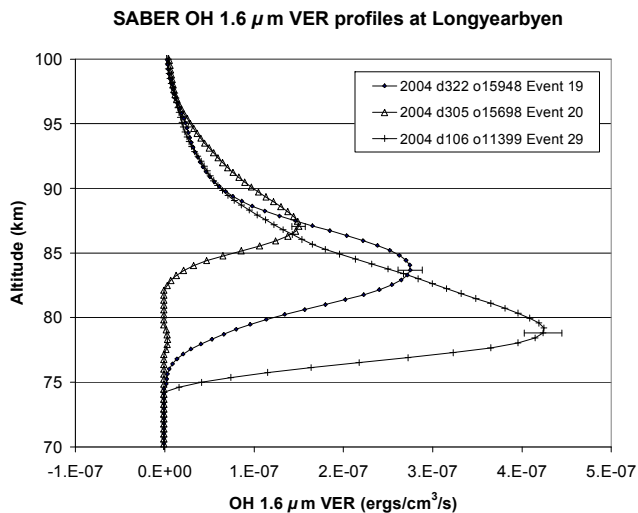


**Fig. 1.** SABER OH  $1.6\ \mu\text{m}$  VER profiles representative of Longyearbyen ( $78\pm 5^\circ\text{N}$ ,  $16\pm 10^\circ\text{E}$ ) in the period 2002–2008. Representative error bars of  $\pm 5\%$  of the maximum in each profile are included. This is the estimated systematic error quoted for OH VER profiles in the altitude range 70–90 km (López-Puertas et al., 2004).

employed in this study. These profiles are calculated from Abel inversions of the SABER limb radiance profile (Lopez-Puertas et al., 2004) followed by correction for instrument spectral response by the use of an “unfilter” factor as described by Mlynczak et al. (2005). The OH-B band channel is sensitive in the range  $1.56\text{--}1.72\ \mu\text{m}$  which includes mostly the OH(4-2) and OH(5-3) bands and was selected in preference to the OH-A channel, which includes mostly the  $\Delta v=2$  bands originating in levels 9 and 8, because the higher vibrational bands tend to have their maxima at higher altitude (Kaufmann et al., 2008). Baker et al. (2007) made use of this channel in their study of equatorial enhancements of the nighttime mesospheric OH airglow layer.

Since the focus of our study was on ground-based measurements made at Longyearbyen, and since longitudinal variations were not ruled out in the investigation by Liu and Shepherd (2006), we restricted ourselves to orbits that satisfied the selection criteria – latitude:  $78\pm 5^\circ\text{N}$ ; longitude:  $16\pm 10^\circ\text{E}$  – corresponding to a radius of about 600 km centred on the station. At these latitudes, the OH-B channel ( $1.56\text{--}1.72\ \mu\text{m}$ ) is susceptible to increased background during enhanced auroral activity arising primarily from  $\text{N}_2$  1P and  $\text{N}_2^+$  Meinel emissions (Gattinger and Vallance Jones, 1981). Part of our investigation was to examine whether an empirical formula of the form reported by Liu and Shepherd (2006) could be established in these conditions.

We restricted ourselves to night time profiles only for which the solar zenith angle (SZA) was greater than  $105^\circ$ . The OH-B wavelength range,  $1.56\text{--}1.72\ \mu\text{m}$ , includes the  $\text{O}_2$  Infrared Atmospheric (0,1) emission at  $1.58\ \mu\text{m}$ , which has a

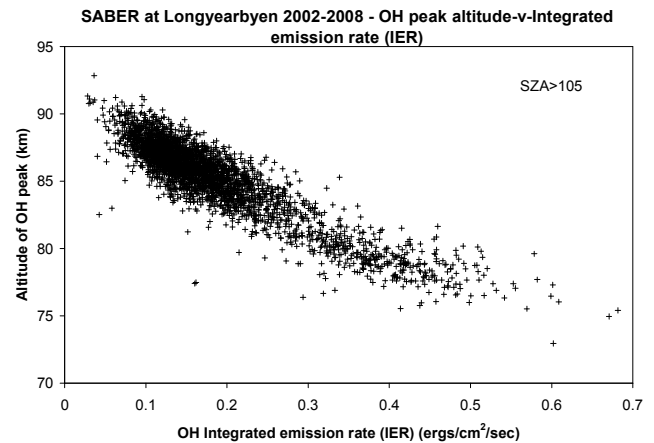


**Fig. 2.** Altitude of OH maximum and integrated emission rate (IER) for each profile measured by SABER at Longyearbyen ( $78\pm 5^\circ\text{N}$ ,  $16\pm 10^\circ\text{E}$ ) in the period 2002–2008, when the solar zenith angle (SZA)  $> 105^\circ$ .

lifetime of  $\sim 3900\ \text{s}$  (Badger et al., 1965). This very long lifetime for an airglow species results in a significant fraction of twilight and early nightglow arising from remnant dayglow excitation, which could contaminate the OH-B VER. This could produce a profile whose maximum value is at an altitude significantly lower than the true maximum of the OH layer. Oxygen  $\text{O}_2(1\Delta_g)$  VER (available in Level 2A SABER data) derived from the SABER  $1.27\ \mu\text{m}$  channel provided a method of assessing the likely contribution of the  $1.58\ \mu\text{m}$  emission to the OH-B channel. The SZA cut-off was chosen on the basis that the day time  $\text{O}_2(1\Delta_g)$  VER had diminished to average nighttime values for  $\text{SZA} > 105^\circ$ . Winick et al. (2009) also used a cut off of  $\text{SZA} > 105^\circ$  in their study of OH layer characteristics during the unusual boreal winters of 2004 and 2006.

Application of the selection criteria given above resulted typically in five or six profiles per day during a northward looking yaw cycle, and over the period January 2002–July 2008, and provided more than 3100 profiles in total. Figure 1 shows three OH  $1.6\ \mu\text{m}$  VER profiles which are representative of the SABER profiles over Longyearbyen during the period 2002–2008, and it illustrates the relationship between the altitude of the OH layer peak and the VER in the layer observed by Liu and Shepherd for WINDII profiles.

Following the method of Liu and Shepherd (2006), the peak altitude of the Gaussian that best fitted the peak of the profile was taken as the altitude of the OH layer peak and the corresponding integrated emission rate (IER) was obtained by computing the integral of the area under the VER profile. We shall use the term SABER OH IER to describe this latter quantity throughout the remainder of the text. Figure 2 is a scatter plot of the peak altitude of each profile versus the SABER OH IER. The inverse relationship between the OH layer peak altitude and the SABER

**Table 1.** Coefficients of the empirical model for the peak altitude of the OH nightglow emission at Longyearbyen. Row 4 gives the coefficients for the empirical formula relating the SABER OH IER,  $I_s$ , to the peak altitude of the OH layer.

row	$h_0$ , km	Term $I_s$		Term $I_s^2$		Term $f$		$\cos(2\pi d/T)$		$\sin(2\pi d/T)$		$\cos(4\pi d/T)$		$\sin(4\pi d/T)$		Population	Standard error $\sigma$ (km)
		$a_1$	$\sigma_1$	$a_2$	$\sigma_2$	$a_3$	$\sigma_3$	$a_4$	$\sigma_4$	$a_5$	$\sigma_5$	$a_6$	$\sigma_6$	$a_7$	$\sigma_7$		
1	90.4	-27.8	0.2	-	-	-	-	-	-	-	-	-	-	-	-	79.9%	1.23
2	90.1	-27.7	0.2	-	-	0.0029	0.0005	-	-	-	-	-	-	-	-	80.3%	1.22
3	91.2	-27.7	0.2	-	-	0.0037	0.0004	-2.1	0.5	0.4	0.1	0.0	0.2	0.2	0.1	83.7%	1.14
4	93.9	-39.7	0.9	23.2	1.6	0.0047	0.0004	-4.6	0.6	0.9	0.1	1.0	0.2	-0.2	0.1	85.0%	1.10

OH IER is immediately apparent. Through the use of multiple linear regression, we examined the influence of the various terms included in the empirical formula reported by Liu and Shepherd, i.e., SABER OH IER,  $I_s$  in ergs/cm<sup>2</sup>/s (the subscript “s” refers to the satellite to distinguish it from spectrometer measurements made from the ground  $I_g$  described in Sect. 2.2), observed 10.7 cm solar flux,  $f$ , in s.f.u. (1 s.f.u.=10<sup>-22</sup> W m<sup>-2</sup> Hz<sup>-1</sup>), annual and semi annual terms as well as diurnal and semidiurnal terms. (The solar flux data was downloaded from the Penticton site at <http://www.wdcb.rssi.ru/stp/data/solar.act/flux10.7/>). Retaining the notation employed by Liu and Shepherd (2006), the empirical model can be expressed as:

$$\begin{aligned}
 h = & h_0 + a_1 I_s + a_2 I_s^2 + a_3 f + a_4 \cos\left(\frac{2\pi d}{T}\right) + a_5 \sin\left(\frac{2\pi d}{T}\right) \\
 & + a_6 \cos\left(\frac{4\pi d}{T}\right) + a_7 \sin\left(\frac{4\pi d}{T}\right) \\
 & + a_8 \cos\left(\frac{2\pi t}{D}\right) + a_9 \sin\left(\frac{2\pi t}{D}\right) \\
 & + a_{10} \cos\left(\frac{4\pi t}{D}\right) + a_{11} \sin\left(\frac{4\pi t}{D}\right) \quad (1)
 \end{aligned}$$

where  $h$  is the peak emission altitude in km,  $h_0$  is a constant term in km,  $d$  is the day number of the year and  $t$  is the local time of the observation,  $T$  and  $D$  are the length of the year in days and the length of the day in hours respectively, and the  $a_i$  are the coefficients of the various terms. By far the most significant term in fitting the peak altitude was the SABER OH IER,  $I_s$ . Next in importance came the annual and semi-annual terms followed by the solar flux term,  $f$  which has only minor importance since the measurements were made in the middle of the Arctic winter. Each of the terms in Eq. (1) was retained on the basis that it satisfied the student T-test for statistical significance in predicting the peak altitude of the OH layer. The fit was improved by including a term in  $I_s^2$  as shown in Table 1. This may be due to the fact that at higher latitudes the OH layer descends by more than one scale height (particularly during the extraordinary spring seasons of 2004 and 2006, when the layer was as low as 76 km on occasions), at which point one might expect some nonlinear response. The rightmost column labelled “population” is a measure of the percentage of predicted altitudes that were within 1.5 km of the actual peak. The values are compara-

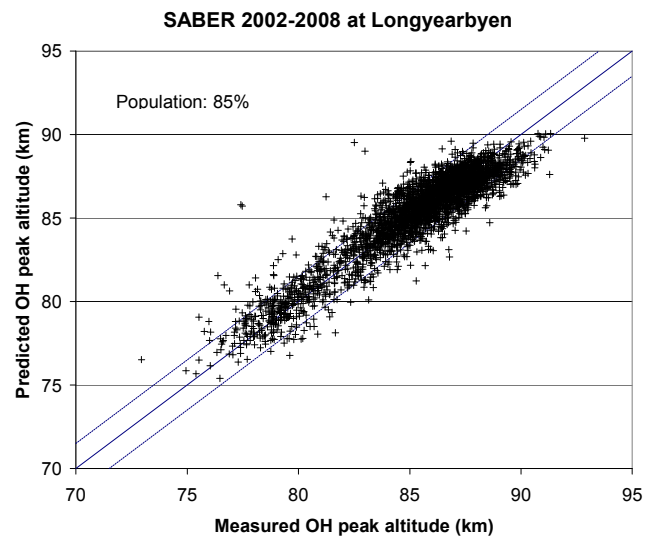


**Fig. 3.** Altitude of OH layer peak predicted by empirical formula versus altitude measured by SABER at Longyearbyen (78±5° N, 16±10° E) during 2002–2008.

ble to the figures reported by Liu and Shepherd (2006) for predictions within ±1 km of the actual peak. The slight reduction in accuracy may be due to the greater excursions of the OH layer at higher latitudes, and that our analysis included peak altitudes for all profiles in contrast to Liu and Shepherd (2006) who excluded profiles that departed from the ideal single peak. We consider that this is a more realistic assessment of the method since a ground-based observer with access only to IER data has no way of knowing when a single peaked OH layer is being observed, or when a more complex profile is present. Figure 3 shows a plot of the modelled OH peak altitude versus the measured values using the coefficients in row 4 of Table 1 in Eq. (1). The right hand column of this table shows the standard error in the peak altitude for the empirical formula used.

The results of this investigation showed that the methodology of Liu and Shepherd (2006) adapted for SABER OH VER profiles observed over Longyearbyen yielded a formula relating the altitude of the OH peak emission to the integrated emission rate. The next step involved finding a relation between the SABER OH IER and the IER of the OH(6-2) band observed by the spectrometer.

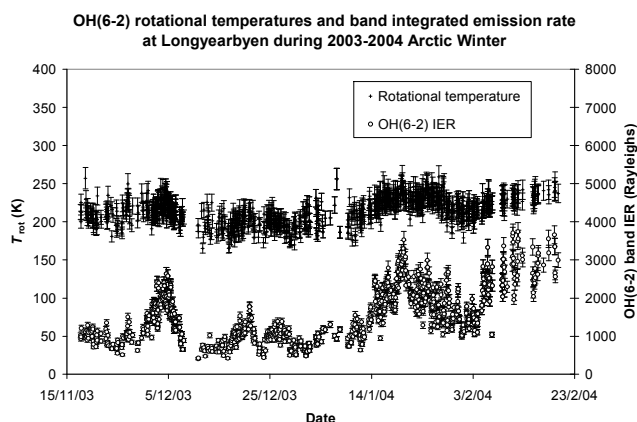


**Fig. 4.** OH(6-2) rotational temperatures and OH(6-2) integrated emission rates measured by the Ebert-Fastie spectrometer at Longyearbyen during the 2003–2004 Arctic winter season.

## 2.2 Ebert-Fastie spectrometer

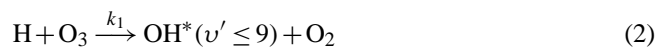
An Ebert-Fastie spectrometer has been deployed at Longyearbyen (78° N, 16° E) for the purpose of studying hydroxyl nightglow emissions in each winter season for over a quarter century (Dyrlund and Sigernes, 2007). The instrument used to obtain the measurements reported here has a 1 m focal length and a field-of-view of approximately 5° viewing in the zenith. Spectra recorded by this instrument have been analysed to derive the rotational temperature of the emitting OH radicals at the emission altitude, e.g., Sivjee and Hamwey (1987), Sigernes et al. (2003), Dyrlund and Sigernes (2007). Detailed descriptions of the spectrometer characteristics, calibration and data reduction techniques are available in Sigernes et al. (2003) and Dyrlund and Sigernes (2007). In addition to the rotational temperature, these spectra have also been used to compute the integrated emission rate (IER) of the observed band, e.g., Myrabø et al. (1983), Myrabø et al. (1987) and Viereck and Deehr (1989). The analysis of each measured spectrum begins with the conversion from counts/channel to Rayleighs/Ångstrom through the use of a calibration function for the instrument described in detail in Dyrlund and Sigernes (2007). The observed spectrum is then fitted with a synthetic spectrum based on the instrument function. The background is determined from the optimal fit between the measured and synthetic spectrum through iteration until the least square error is minimal and is then removed. Finally, the temperature is determined from the slope of the linear fit to a Boltzmann plot of the P<sub>1</sub>(2), P<sub>1</sub>(3) P<sub>1</sub>(4) and P<sub>1</sub>(5) lines of the OH(6-2) band. The P<sub>2</sub> lines must also follow the same linear fit as otherwise, the emitting radicals are not in thermal equilibrium. Results for a particular spectrum are accepted only when it satisfies the following criteria:

1. the variance of linear fit to the Boltzmann plot of the P<sub>1</sub> and P<sub>2</sub> lines is consistent with thermal equilibrium of the emitting radicals (var P<sub>1</sub> < 0.05 and var P<sub>2</sub> < 0.3);
2. auroral contamination (particularly OI 8446 Å line) is below the threshold that would adversely affect the determination of temperature (intensity of 8446 line not more than twice the intensity of the OH P<sub>1</sub>(3) line);
3. the background is below the threshold count established to eliminate spectra contaminated by moonlight and/or clouds.

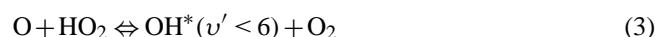
The application of these criteria eliminates ~46% of spectra. Once the temperature has been determined, the IER of the band is determined by integrating the total signal under the best fit synthetic profile. We shall refer to these values as OH(6-2) IER. Of particular relevance here is the elimination of spectra that are affected to a significant degree by atmospheric extinction. Based on the observations of Myrabø and Deehr (1984), it is unlikely that the selection criteria are capable of eliminating spectra that have less than 20% reduction in band radiance due to atmospheric extinction. In Sect. 4 we consider the impact that such a reduction would have on the OH peak altitude assigned. Instrument calibration takes account of variations in the spectrometer sensitivity across the spectral interval accepted by the spectrometer. Long term stability is monitored by the use of calibration lamp as described in Dyrlund and Sigernes (2007). In common with the temperature data from the spectrometer, OH(6-2) IER values are calculated on an hourly average basis. Figure 4 shows a plot of rotational temperature and OH(6-2) IER values obtained from the OH(6-2) band for the 2003–2004 Arctic winter season at Longyearbyen. The Langhoff et al. (1986) transition probabilities were selected for generating the synthetic spectra used in this report based on the detailed study of the OH(6-2) band by French et al. (2000).

## 2.3 Relating OH(6-2) IER to SABER OH IER values

The OH(6-2) IERs from the ground-based Ebert-Fastie spectrometer provide a record of the time variation of the OH(6-2) band emission, whereas the IER values calculated from SABER provide the corresponding record for the sum of the OH(4-2) and (5-3) bands. It is generally accepted that the reaction



with  $k_1 = 1.4 \times 10^{-10} e^{-480/T} \text{ cm}^3 \text{ s}^{-1}$  is the primary source of vibrationally excited OH. The reaction



is sometimes considered to be a secondary source for vibrational levels ( $v' \leq 6$ ), but overall this reaction is believed to be of minor importance during night time conditions (Makhlouf

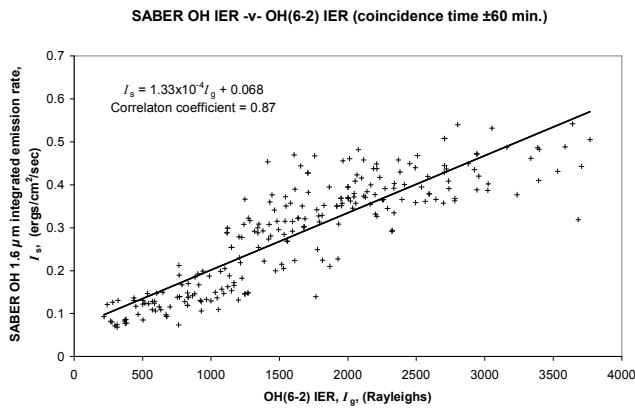
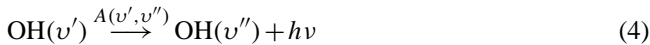
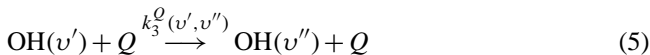


**Fig. 5.** Scatter plot of integrated emission rates (IER) measured by SABER at Longyearbyen ( $78\pm 5^\circ$  N,  $16\pm 10^\circ$  E) together with OH(6-2) IER measured by the Ebert-Fastie ground-based spectrometer during the period when the two sets of measurements overlap (16 January 2004–19 February 2004). The time window for coincidence of the two sets of data is  $\pm 60$  min.

et al., 1995). Since the OH products of Reaction (2) are found in vibrational levels 6, 7, 8 and 9 (Kaufmann et al., 2008), lower vibrational levels are populated as a result of radiative cascade



and single or multi-quantum, collisional deactivation (McDade and Llewellyn, 1987)



OH bands arising from different initial ( $v'$ ) and final ( $v''$ ) vibrational states have different average IERs as reported by Krassovsky et al. (1962) with updated values for some of these bands by Cosby and Slanger (2007). However, it is believed that the relative variations of IERs from adjacent upper states follow each other closely due to the common origin of their primary source. Wrasse et al. (2004) show a number of nights with good correspondence between the IER of the OH(8-3) and (6-2) bands at  $23^\circ$  S. Mulligan et al. (1995) found very good agreement between variations in the OH(4-2) and (3-1) bands at  $53^\circ$  N. Based on these observations, we assume that the relative variations in the OH(6-2), (5-3) and (4-2) IERs follow one another closely. This enabled us to establish a relation between the OH(6-2) IER measured by the ground-based spectrometer,  $I_g$ , and the SABER OH IER for the  $1.6 \mu\text{m}$  band,  $I_s$ , calculated from SABER profiles.

The yaw cycle for SABER is such that it is looking southward during the middle of the Arctic winter (mid-November to mid-January). Fortunately, a remarkable period of good observing conditions during the winter of 2004 provided 35 days of ground-based OH measurements during a time when SABER was looking northward. Table 2 shows the

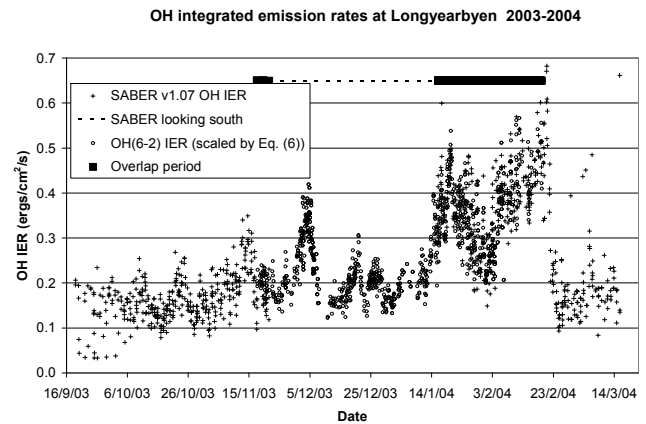


**Fig. 6.** Integrated emission rates (IER) calculated from SABER profiles at Longyearbyen ( $78\pm 5^\circ$  N,  $16\pm 10^\circ$  E) together with OH(6-2) IERs measured by the Ebert-Fastie during 2003–2004 season. The OH(6-2) IER values have been scaled according to the relationship illustrated in Fig. 5.

results of applying different time coincidence criteria to the SABER and ground-based IER measurements. As expected, the number of coincidences increases as the time window is expanded. Each coincidence set of measurements was fitted with a best fit line of the form

$$I_s = m I_g + c \quad (6)$$

in the least squares sense, from which the slope,  $m$ , constant,  $c$ , and correlation coefficient,  $r$ , were determined. The results of these fits are also shown in Table 2. Since OH(6-2) spectra that include auroral contamination have been omitted from the comparison, and since we use coincidence criteria to select SABER and OH(6-2) IER measurements for the comparison, we expect that the majority of measurements contaminated by aurora will have been removed. Figure 5 is a scatter plot of OH(6-2) IER versus SABER OH IER rates during the 35 day overlap period (16 January 2004–19 February 2004). For the purpose of this plot, a ground-based measurement that occurred within  $\pm 60$  min of a satellite measurement was considered coincident with it. The equation of the best fit line to the data in Fig. 5 ( $I_s = 1.33 \times 10^{-4} I_g + 0.068$ ) was used to relate OH(6-2) IER values,  $I_g$ , to SABER OH IER values,  $I_s$ . A correlation coefficient of 0.87 for the fit indicates the high degree of correspondence between the two data sets. The offset of 0.068 in the best fit line is indicative of some residual auroral background contamination in the SABER IER values. We do not attempt to remove this background, since it is already included in the determination of the coefficients in Eq. (1).

Figure 6 shows the result of combining SABER OH IER,  $I_s$ , with the OH(6-2) IER,  $I_g$  which have been re-scaled according to Eq. (6) ( $I_s = 1.33 \times 10^{-4} I_g + 0.068$ ) for the 2003–2004 season at Longyearbyen. The correspondence between the ground-based and satellite measurements during

**Table 2.** Coincidence criteria used to relate SABER OH IER,  $I_s$ , to OH(6-2) IER  $I_g$ . A linear equation of the form  $I_s = mI_g + c$  was fitted to each coincidence set. Values of  $m$ ,  $c$  and the correlation coefficient,  $r$ , are shown in the table.

Spatial		Time	Number of coincidences	linear fit		Correlation coefficient, $r$
Latitude	Longitude			slope, $m$	constant, $c$	
75±5° N	16±10° E	±15 min	79	1.46×10 <sup>-4</sup>	0.057	0.75
75±5° N	16±10° E	±30 min	145	1.36×10 <sup>-4</sup>	0.066	0.84
75±5° N	16±10° E	±60 min	238	1.33×10 <sup>-4</sup>	0.068	0.87
75±5° N	16±10° E	±120 min	307	1.30×10 <sup>-4</sup>	0.071	0.86

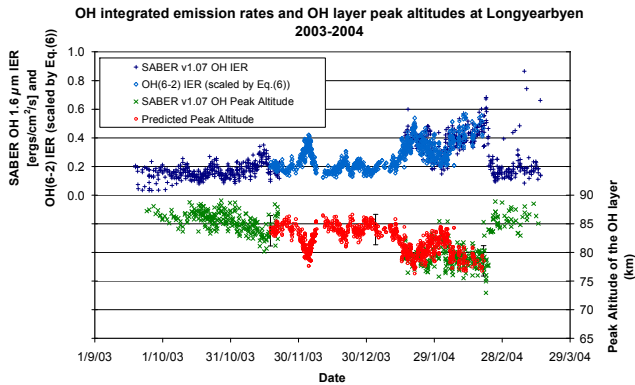


**Fig. 7.** OH layer peak height measured by SABER at Longyearbyen (78±5° N, 16±10° E) (green) and OH layer peak height predicted by empirical formula for all OH(6-2) data (red) (including the period when SABER was looking south) during the 2003–2004 season. The error bar shown in black indicates the uncertainty (±2.7 km) in the peak altitudes determined. SABER OH IER and OH(6-2) IER values (blue) are also shown in this plot to illustrate the inverse relationship between OH brightness and peak altitude.

the overlap period is clearly evident. The standard error in the linear fit obtained from Fig. 5 contributed an uncertainty of ±2.1 km to the modelled values of peak altitude. We note that the overlap period occurred at a time when SABER OH IER values were among the highest observed during the entire seven year period (see Fig. 2). The good agreement between the two data sets in Fig. 6 in the period 17–19 November 2003, during a 3-day period of data overlap when both OH IER values were near the average value, is reassuring.

### 3 Results and discussion

In order to predict the OH peak altitude from the ground-based OH(6-2) IER measurements (in Rayleighs), we substituted for  $I_s$  in Eq. (1) by  $1.33 \times 10^{-4} I_g + 0.068$ . This enabled the peak altitude of the OH layer to be calculated from the measured OH(6-2) IER (in Rayleighs) at a particular time and date and the solar flux value (in s.f.u.) for that date. Figure 7 shows a plot of the OH peak altitude predicted by this technique compared with values of the OH peak al-

titude measured from SABER OH VER profiles. The correspondence between measured and predicted values during the two overlap periods is excellent. More important however is the fact that we now have values for the altitude of the OH layer peak when no SABER profiles are available.

We now attempt to quantify the uncertainties associated with the inferred altitudes. These arise from the two steps in the empirical procedure described above and from the effect of atmospheric extinction. The standard error on the prediction of the OH peak altitude from the SABER OH IER was ±1.1 km, whereas the standard error on the conversion from OH(6-2) IER to SABER OH IER was ±2.1 km. Based on the observations of Myrabø and Deehr (1984), we estimated a maximum reduction of 20% in the IER due to atmospheric extinction in the lower atmosphere. Such a reduction would give rise to an increase of 1.2 km in the assignment of the OH peak altitude using the combined empirical formula. The uncertainties from the two fitting processes and atmospheric extinction resulted in a combined uncertainty of ±2.7 km on each altitude determined. Based on the range of OH peak altitude which extended from 76 km to 90 km in the period 2002–2008, this is a considerable improvement on the nominal 87 km altitude alone. The combined uncertainty is comparable with the ±2.6 km figure quoted originally by Baker and Stair (1988) for the altitude of the OH layer. We estimate that the uncertainty could be reduced to ~2 km with the use of longer periods of overlap of satellite and ground measurements together with simultaneous on-site atmospheric extinction data.

### 4 Conclusion

We have successfully implemented the method suggested by Liu and Shepherd (2006) for estimating the altitude of the OH nightglow emission altitude for a ground-based station. Substituting WINDII profiles of the OH(8-3) P<sub>1</sub>(3) line by SABER OH 1.6 μm VER profiles, we have extended the range of latitudes available from WINDII to include a station as far north as Longyearbyen (78° N). Results are presented for the 2003–2004 winter season, which provided an opportunity to test the method. Assuming a simple correlation between SABER OH IER and OH(6-2) IER measurements, we

have demonstrated that the peak altitude of the OH layer can be modelled to within an uncertainty of  $\pm 2.7$  km. This is comparable with the  $\pm 2.6$  km uncertainty associated with the nominal altitude of the OH layer. On the basis of the stability of the empirical formula over the seven years of available SABER data, it would appear that once established at a particular station, the method provides the ground-based observer with a parameter that was previously unavailable.

*Acknowledgements.* We are very appreciative of the high quality of the SABER measurements and we extend our thanks to the entire SABER/TIMED team for making the data freely available. The report has benefited greatly from the recommendations of the two referees consulted by the journal. We also thank R. P. Lowe of The University of Western Ontario, Canada for his comments on an earlier version of the manuscript.

Topical Editor C. Jacobi thanks G. Shepherd and R. Nijcejewski for their help in evaluating this paper.

## References

- Badger, R. M., Wraight, A. C., and Whitlock, R. F.: Absolute intensities of the discrete and continuous absorption bands of oxygen gas at 1.26 and 1.065  $\mu\text{m}$  and the radiative lifetime of the  $^1\Delta_g$  state of oxygen, *J. Chem. Phys.*, 43, 4345–4350, 1965.
- Baker, D. J., Thurgood, B. K., Harrison, W. K., Mlynczak, M. G., and Russell, J. M.: Equatorial enhancement of the nighttime OH mesospheric infrared airglow, *Phys. Scr.*, 75, 615–619, doi:10.1088/0031-8949/75/5/004, 2007.
- Baker, D. J. and Stair Jr., A. T.: Rocket measurements of the altitude distributions of the hydroxyl airglow, *Physica Scripta*, 37, 611–622, 1988.
- Cosby, P. C. and Slanger, T. G.: OH spectroscopy and chemistry investigated with astronomical sky spectra, *Can. J. Phys.*, 85, 77–99, doi:10.1139/P06-088, 2007.
- Dyrland, M. E. and Sigernes, F.: An update on the hydroxyl airglow temperature record from the Auroral Station in Adventdalen, Svalbard (1980–2005), *Can. J. Phys.*, 85(2), 143–151, doi:10.1139/P07-040, 2007.
- French, W. J. R., Burns, G. B., Finlayson, K., Greet, P. A., Lowe, R. P., and Williams, P. F. B.: Hydroxyl (6-2) airglow emission intensity ratios for rotational temperature determination, *Ann. Geophys.*, 18, 1293–1303, 2000, <http://www.ann-geophys.net/18/1293/2000/>.
- Gattinger, R. L. and Vallance Jones, A.: Quantitative spectroscopy of the aurora. V. The spectrum of strong aurora between 10 000 and 16 000  $\text{\AA}$ , *Can. J. Phys.*, 59, 480–487, 1981.
- Hall, C. M., Aso, T., Tsutsumi, M., Höffner, J., and Sigernes, F.: Multi-instrument derivation of 90 km temperatures over Svalbard (78° N 16° E), *Radio Sci.*, 39, RS6001, doi:10.1029/2004RS003069, 2004.
- Hall, C. M., Aso, T., Tsutsumi, M., Hoffner, J., Sigernes, F., and Holdsworth, D. A.: Neutral air temperatures at 90 km and 70° N and 78° N, *J. Geophys. Res.*, 111, D14105, doi:10.1029/2005JD006794, 2006.
- Hocking, W. K., Argall, P. S., Lowe, R. P., Sica, R. J., and Ellinger, H.: height-dependent meteor temperatures and comparisons with lidar and OH measurements, *Can. J. Phys.*, 85(2), 173–187, doi:10.1139/P07-038, 2007.
- Kaufmann, M., Lehmann, C., Hoffmann, L., Funke, B., López-Puertas, M., von Savigny, C., and Riese, M.: Chemical heating rates derived from SCIAMACHY vibrationally excited OH limb emission spectra, *Adv. Space Res.*, 41, 1914–1920, doi:10.1016/j.asr.2007.07.045, 2008.
- Krassovsky, V. I., Shefov, N. N., and Yarin, V. I.: Atlas of the airglow spectrum 3000–12400  $\text{\AA}$ , *Planet. Space Sci.*, 9, 883–915, 1962.
- Kubota, M., Ishii, M., Shiokawa, K., Ejiri, M. K., and Ogawa, T.: Height measurements of nightglow structures observed by all-sky imagers, *Adv. Space Res.*, 24, 593–596, 1999.
- Kumar, K. K., Vineeth, C., Antonita, T. M., Pant, T. K., and Sridharan, R.: Determination of day-time OH emission heights using simultaneous meteor radar, day-glow photometer and TIMED/SABER observations over Thumba (8.5° N, 77° E), *Geophys. Res. Lett.*, 35, L18809, doi:10.1029/2008GL035376, 2008.
- Langhoff, S. R., Werner, H.-J., and Rosmus, P.: Theoretical transition probabilities for the OH Meinel system, *J. Molec. Spectrosc.*, 118, 507–529, 1986.
- Liu, G. and Shepherd, G. G.: An empirical model for the altitude of the OH nightglow emission, *Geophys. Res. Lett.*, 33, L09805, doi:10.1029/2005GL025297, 2006.
- López-Puertas, M., García-Comas, M., Funke, B., Picard, R. H., Winick, J. R., Wintersteiner, P. P., Mlynczak, M. G., Mertens, C. J., Russell III, J. M., and Gordley, L. L.: Evidence for an OH( $v$ ) excitation mechanism of CO<sub>2</sub> 4.3  $\mu\text{m}$  nighttime emission from SABER/TIMED measurements, *J. Geophys. Res.*, 109, D09307, doi:10.1029/2003JD004383, 2004.
- Makhlouf, U. B., Picard, R. H., and Winick, J. R.: Photochemical-dynamical modeling of the measured response of airglow to gravity waves 1. Basic model for OH airglow, *J. Geophys. Res.*, 100(D6), 11289–11311, 1995.
- McDade, I. C. and Llewellyn, E. J.: Kinetic parameters related to sources and sinks of vibrationally excited OH in the nightglow, *J. Geophys. Res.*, 92, 7643–7650, 1987.
- Mertens, C. J., Schmidlin, F. J., Goldberg, R. A., Remsberg, E. E., Pesnell, W. D., Russell III, J. M., Mlynczak, M. G., López-Puertas, M., Wintersteiner, P. P., Picard, R. H., Winick, J. R., and Gordley, L. L.: SABER observations of mesospheric temperatures and comparisons with falling sphere measurements taken during the 2002 summer MacWAVE campaign, *Geophys. Res. Lett.*, 31, L03105, doi:10.1029/2003GL018605, 2004.
- Mlynczak, M. G., Martin-Torres, F. J., Crowley, G., et al.: Energy transport in the thermosphere during the solar storms of April 2002, *J. Geophys. Res.*, 110, A12S25, doi:10.1029/2005JA011141, 2005.
- Myrabø, H. K., Deehr, C. S., and Sivjee, G. G.: Large-amplitude nightglow OH(8-3) band intensity and rotational temperature variations during a 24-hour period at 78° N, *J. Geophys. Res.*, 88(A11), 9255–9259, 1983.
- Myrabø, H. K. and Deehr, C. S.: Mid-winter hydroxyl night airglow emission intensities in the northern polar region, *Planet. Space Sci.*, 32, 263–271, 1984.
- Myrabø, H. K., Deehr, C. S., and Viereck, R.: Polar mesopause gravity wave activity in the sodium and hydroxyl night airglow, *J. Geophys. Res.*, 92(A3), 2527–2534, 1987.
- Mulligan, F. J., Horgan, D. F., Galligan, J. M., and Griffin, E. M.: Mesopause temperatures and integrated band brightnesses

- calculated from airglow OH emissions recorded at Maynooth (53.2° N, 6.4° W) during 1993, *J. Atmos. Terr. Phys.*, 57, 1623–1637, 1995.
- Oberheide, J., Offermann, D., Russell III, J. M., and Mlynczak, M. G.: Intercomparison of kinetic temperature from 15  $\mu\text{m}$  CO<sub>2</sub> limb emissions and OH\*(3, 1) rotational temperature in nearly coincident air masses: SABER, GRIPS, *Geophys. Res. Lett.*, 33, L14811, doi:10.1029/2006GL026439, 2006.
- Sigernes, F., Shumilov, N., Deehr, C. S., Nielsen, K. P., Svenøe, T., and Havnes, O.: Hydroxyl rotational temperature record from the auroral station in Adventdalen, Svalbard (78° N, 15° E), *J. Geophys. Res.*, 108(A9), 1342, doi:10.1029/2001JA009023, 2003.
- Sivjee, G. G. and Hamwey, R. M.: Temperature and chemistry of the polar mesopause OH, *J. Geophys. Res.*, 92(A5), 4663–4672, 1987.
- Sivjee, G. G., Walterscheid, R. L., Hecht, J. M., Hamwey, R. M., Schubert, G., and Christensen, A. B.: Effects of Atmospheric Disturbances on Polar Mesopause Airglow OH emissions, *J. Geophys. Res.*, 92(A7), 7651–7656, 1987.
- She, C. Y. and Lowe, R. P.: Seasonal temperature variations in the mesopause region at mid-latitude: comparison of lidar and hydroxyl rotational temperatures using WINDII/UARS OH height profiles, *J. Atmos. Solar Terr. Phys.*, 60(16), 1573–1583, 1998.
- Takahashi, H., Wrasse, C. M., Gobbi, D., Nakamura, T., Shiokawa, K., and Lima, L. M.: Airglow OH emission height inferred from OH temperature and meteor trail diffusion coefficient, *Adv. Space Res.*, 35, 1940–1944, 2005.
- Viereck, R. A. and Deehr, C. S.: On the interaction between gravity waves and the OH Meinel (6-2) and the O<sub>2</sub> atmospheric (0-1) bands in the polar night airglow, *J. Geophys. Res.*, 94, 5397–5404, 1989.
- Winick, J. R., Wintersteiner, P. P., Picard, R. H., Esplin, D., Mlynczak, M. G., Russell III, J. M., and Gordley, L. L.: OH layer characteristics during unusual boreal winters of 2004 and 2006, *J. Geophys. Res.*, 114, A02303, doi:10.1029/2008JA013688, 2009.
- Wrasse, C. M., Takahashi, H., and Gobbi, D.: Comparison of the OH (8-3) and (6-2) band rotational temperature of the mesospheric airglow emissions, *Rev. Bras. Geof. (online)*, 22(3), 223–231, ISSN 0102-261X, doi:10.1590/S0102-261X2004000300002, 2004.
- Yee, J.-H., Crowley, G., Roble, R. G., Skinner, W. R., Burrage, M. D., and Hays, P. B.: Global simulations and observations of O(<sup>1</sup>S), O<sub>2</sub>(<sup>1</sup>Σ) and OH mesospheric nightglow emissions, *J. Geophys. Res.*, 102(A9), 19949–19968, 1997.